Ultrasound in Medicine & Biology 49 (2023) 2264–2272

Contents lists available at ScienceDirect

Ultrasound in Medicine & Biology

journal homepage: www.elsevier.com/locate/ultrasmedbio

Original Contribution

Ultrasound Shear Wave Attenuation Imaging for Grading Liver Steatosis in Volunteers and Patients With Non-alcoholic Fatty Liver Disease: A Pilot Study

Ladan Yazdani [a,b], Iman Rafati [a,b], Marc Gesnik [a], Frank Nicolet [a], Boris Chayer [a], Guillaume Gilbert [c,d], Anton Volniansky [d], Damien Olivié [d], Jeanne-Marie Giard [e], Giada Sebastiani [f], Bich N. Nguyen [g], An Tang [d,h], Guy Cloutier [a,b,d,*]

[a] Laboratory of Biorheology and Medical Ultrasonics (LBUM), Centre de recherche du Centre hospitalier de l'Université de Montréal (CRCHUM), Montréal, QC, Canada
[b] Institute of Biomedical Engineering, Université de Montréal, Montréal, QC, Canada
[c] MR Clinical Science, Philips Healthcare Canada, Markham, ON, Canada
[d] Department of Radiology, Radiation Oncology and Nuclear Medicine, Université de Montréal, Montréal, QQ, Canada
[e] Department of Hepatology, Université de Montréal, Montréal, QC, Canada
[f] Division of Gastroenterology and Hepatology, McGill University Health Centre, Montreal, QC, Canada
[g] Service of Pathology, Centre Hospitalier de l'Université de Montréal (CHUM), Montréal, QC, Canada
[h] Laboratory of Clinical Image Processing, CRCHUM, Montréal, QC, Canada

ARTICLE INFO

Keywords:
Ultrasound
Shear wave
Elastography
Attenuation
Dispersion
Magnetic resonance imaging proton density fat fraction
Biopsy
Liver steatosis
Cutoff threshold
Non-alcoholic fatty liver disease

Objective: The aims of the work described here were to assess shear wave attenuation (SWA) in volunteers and patients with non-alcoholic fatty liver disease (NAFLD) and compare its diagnostic performance with that of shear wave dispersion (SWD), magnetic resonance imaging (MRI) proton density fat fraction (PDFF) and biopsy.
Methods: Forty-nine participants (13 volunteers and 36 NAFLD patients) were enrolled. Ultrasound and MRI examinations were performed in all participants. Biopsy was also performed in patients. SWA was used to assess histopathology grades as potential confounders. The areas under curves (AUCs) of SWA, SWD and MRI-PDFF were assessed in different steatosis grades by biopsy. Youden's thresholds of SWA were obtained for steatosis grading while using biopsy or MRI-PDFF as the reference standard.
Results: Spearman's correlations of SWA with histopathology (steatosis, inflammation, ballooning and fibrosis) were 0.89, 0.73, 0.62 and 0.31, respectively. Multiple linear regressions of SWA confirmed the correlation with steatosis grades (adjusted $R^2 = 0.77$, $p < 0.001$). The AUCs of MRI-PDFF, SWA and SWD were respectively 0.97, 0.99 and 0.94 for S0 versus ≥S1 ($p > 0.05$); 0.94, 0.98 and 0.78 for ≤S1 versus ≥S2 (both MRI-PDFF and SWA were higher than SWD, $p < 0.05$); and 0.90, 0.93 and 0.68 for ≤S2 versus S3 (both SWA and MRI-PDFF were higher than SWD, $p < 0.05$). SWA's Youden thresholds (Np/m/Hz) (sensitivity, specificity) for S0 versus ≥S1, ≤S1 versus ≥S2 and ≤S2 versus S3 were 1.05 (1.00, 0.92), 1.37 (0.96, 0.96) and 1.51 (0.83, 0.87), respectively. These values were 1.16 (1.00, 0.81), 1.49 (0.91, 0.82) and 1.67 (0.87, 0.92) when considering MRI-PDFF as the reference standard.
Conclusion: In this pilot study, SWA increased with increasing steatosis grades, and its diagnostic performance was higher than that of SWD but equivalent to that of MRI-PDFF.

Introduction

Non-alcoholic fatty liver disease (NAFLD) is the most prevalent liver disease, particularly in Western nations [1], and it is a leading cause of liver-related morbidity and mortality [2]. This disease is associated with metabolic impairments such as obesity and type 2 diabetes mellitus [3]. NAFLD may develop into a progressive form, non-alcoholic steatohepatitis (NASH), which may lead to fibrosis, cirrhosis and cancer. Therefore, early identification is important to prevent progression and reduce overall mortality [4].

Although liver biopsy is recognized as the historical reference standard for assessment of NAFLD and for the definite diagnosis of NASH [5,6], there are some limitations, including sampling inaccuracy, low patient acceptance (especially for disease monitoring) and the risk of bleeding [7–9]. Therefore, the acceptability of biopsy for screening on a wide scale and for longitudinal disease monitoring is limited [10,11].

* Corresponding author. Laboratory of Biorheology and Medical Ultrasonics, University of Montreal Hospital Research Center, 900 Saint-Denis, Room R11-464, Montreal, Quebec, Canada, H2X 0A9.
E-mail address: guy.cloutier@umontreal.ca (G. Cloutier).

https://doi.org/10.1016/j.ultrasmedbio.2023.06.020
Received 31 March 2023; Revised 26 June 2023; Accepted 27 June 2023

Different imaging methods have been investigated to quantitate steatosis non-invasively [12–14]. Magnetic resonance imaging (MRI)-based techniques have been developed to measure the proton density fat fraction (PDFF), a biomarker of steatosis, with good precision and reproducibility [15,16]. The MRI-PDFF method has been reported to detect steatosis with higher sensitivity than B-mode ultrasound (US) [13,16,17]. However, MRI is costly, has more limited availability and is not available as a point-of-care device [13,18]. MRI is also impractical for large-scale screening when considering the high prevalence of NAFLD [16,19]. Computed tomography (CT) can be used for steatosis detection. However, except for opportunistic screening when CT is performed for another indication, it is generally not suitable as a screening method because of the concerns over ionizing radiation [20].

B-Mode US can be used to grade steatosis semi-quantitatively on the basis of increased backscatter (higher echogenicity), attenuation and image clutter. However, assessment is operator dependent with moderate agreement between readers [21], the sensitivity is low for detection of mild steatosis [22], the steatosis grading ability is limited [23] and the performance drops markedly in morbidly obese patients [24]. Building on the success of shear wave elastography (SWE) [25] for quantifying and staging fibrosis [26], some US techniques have been proposed for liver fat quantification. A study explored experimentally the link between shear wave dispersion (SWD) and shear wave attenuation (SWA), which are both related to tissue viscosity [27]. Moreover, studies have found that SWD and SWA correlate with steatosis grades [27–31]. Also, SWA related to the lossy nature of tissues [29,32,33] was found to vary with the fat content, according to pre-clinical fatty duck liver experiments [29]. However, few studies have assessed the feasibility and diagnostic performance of SWA in the context of NAFLD [27,31,33].

The purpose of this pilot study was to assess SWA in volunteers and patients with NAFLD. Secondary aims were to assess potential confounders, compare its diagnostic performance for grading steatosis with SWD and MRI-PDFF and identify diagnostic thresholds when using either histopathology or MRI-PDFF as the reference standard.

Methods

Design and participants

This single-site, prospectively designed, cross-sectional imaging trial was undertaken to evaluate the diagnostic accuracy of shear wave (SW) techniques in non-obese volunteers and patients, using histopathology as the reference standard for patients. This study was approved by the institutional review board of the Centre de recherche du Centre Hospitalier de l'Université de Montréal (CRCHUM). All participants gave their written informed consent.

Between January 2020 and May 2023, normal volunteers and patients were enrolled to obtain a representative spectrum of disease. Non-NAFLD volunteers were included if they were adults with no risk factors for developing liver steatosis (including type 2 diabetes mellitus, alcohol consumption >60 g of alcohol per day, lipogenic medication and body mass index [BMI] >25 kg/m^2) and had no liver steatosis (defined as MRI-PDFF <5%). Those with NAFLD were included if they were adults with suspected or known NAFLD or NASH who had to undergo a liver biopsy as part of their clinical standard of care. Subjects were excluded if they had other causes of chronic liver disease or had undergone a liver transplant. Contra-indications to MRI (such as claustrophobia and pacemaker) did not constitute an exclusion criterion because the primary endpoint was the diagnostic accuracy of SW US according to biopsy. Figure 1 is the flowchart of patient enrollment.

US data acquisition

A Verasonics Vantage programmable system (Verasonics Inc., Kirkland, WA, USA) and a 128-element curved array US transducer (ATL C5-2, Philips Healthcare, Andover, MA, USA) were used to generate acoustic radiation force push beams and track induced displacements. Details on the US sequence used, US SW generation and tracking and intensity measurements respecting acoustic output standards are provided in Supplement S1 (online only). To visualize the SW propagation and confirm image quality, a cine-loop reconstruction was done immediately after the acquisition. Then, the beamforming was done using the f-k migration method [34] on acquired data by compounding the coherent sum of three angled planes between −1 and 1°.

US data post-processing

A 2-D autocorrelation algorithm [35] applied to radiofrequency (RF) data was used to display the SW velocity field. The polar coordinates of acquired data were converted in Cartesian coordinates for further processing. The region of interest (ROI) for each acquisition was selected 3 mm away on the right of the last SW push line. Each ROI had a width of 1.5 cm and a length of 1.2 cm, which corresponds to the length of the acoustic radiation force push line in the depth direction, or smaller in the cases in which the segmented contour had a smaller size because of high noise. All processing was done in MATLAB (Version 2018a, The MathWorks, Natick, MA, USA). SWA was computed based on the revisited frequency shift (R-FS) method [33]. The SWA was computed over the whole amplitude spectrum frequency range 0–1000 Hz. SWD was estimated as the slope of the SW phase velocity-versus-frequency curve, according to [28,36], on the same ROI as SWA computations by averaging the velocity field over depth. The A-RANSAC method inspired by Yazdani et al. [33] was used for line fitting and for finding the slope. The SWD was computed between averaged values of the lower frequency at half-maximum (67 Hz) and peak frequency (110 Hz), determined *a posteriori* on the whole data set. For more details on SWA and SWD computation, readers are referred to Supplement S2 (online only).

MRI examination

The MRI-PDFF was measured using the Achieva TX 3T MRI system (Philips Healthcare, Best, Netherlands). A two-channel body coil and a 16-channel surface array coil were used for transmission and signal reception. The software versions were R5.3.1 (January 2020–September 2020), R5.6.1 (September 2020–November 2022) and R5.7.1 (November 2022–May 2023), and the sequence was a 3-D chemical shift-encoded multi-echo gradient-echo sequence using six echoes (mDixon Quant). A multifrequency spectral fat model and a T2* correction were used to perform the water/fat separation in the complex domain. Also, to avoid T1 bias, a low flip angle of 3° was used. The ratio of fat proton density to total fat and water proton density provided the PDFF [15,37]. MRI-PDFF analysis was performed using OsiriX MD Version 9.0.2 by a medical student under the supervision of an experienced radiology investigator. A single slice of the liver was chosen for segmentation at a level where the spleen was well visible and hepatic veins less prominent. The region of interest included left and right livers and excluded the inferior vena cava and Glisson's capsule.

Histological analysis of tissue samples

For patients, liver biopsies were obtained with 16- or 18-gauge needles in the right liver lobe using an intercostal approach for clinical care or NASH Clinical Research Network (CRN) procedures. Hematoxylin and eosin, periodic acid–Schiff, periodic acid–Schiff–diastase, reticulin and Masson's trichrome stains were used [38]. As chronic liver disease is diffuse, the location of the biopsies was not correlated with that of the US or MRI quantitative measurements. An expert hepato-pathologist (B.N. N.) analyzed histology slides and applied the NASH-CRN scoring system [8]. Steatosis was graded from 0 to 3 (S0 to S3), lobular inflammation was graded from 0 to 3 (I0 to I3), hepatocellular ballooning was graded from 0 to 2 (B0 to B2) and fibrosis was staged from 0 to 4 (F0 to F4).

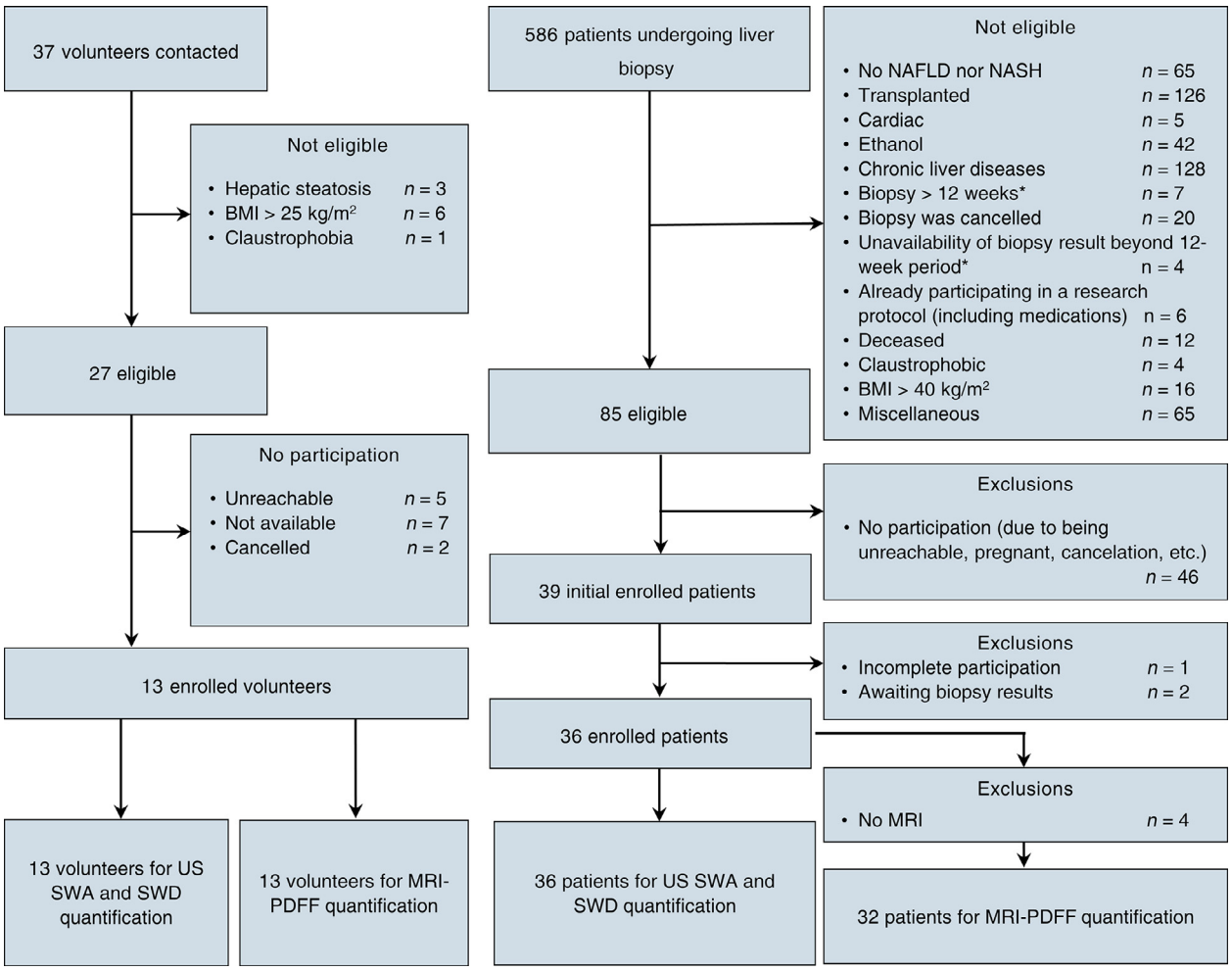

Figure 1. Flowchart of the participant enrollment process. BMI, body mass index; MRI-PDFF, magnetic resonance imaging proton density fat fraction; NAFLD, non-alcoholic fatty liver disease; NASH, non-alcoholic steatohepatitis; SWA, shear wave attenuation; SWD, shear wave dispersion; US, ultrasound.

Statistical analysis

Means and standard deviations (SD) of SWE parameters were reported for each imaging session. When the Shapiro–Wilk normality test failed, a non-parametric Kruskal–Wallis rank sum test was used to determine SWA statistical differences between histopathology grades, and corresponding p values were reported. A *post hoc* Dunn test was used for multiple pairwise comparisons between histopathological grades and stages.

Linear regressions were used to determine the relationship between SWA measurements and MRI-PDFF values, or liver biopsy grades. As histopathology grades are semiquantitative, the non-parametric Spearman rank correlation coefficient was used to assess strengths of correlations between SWA and liver biopsy grades, age, BMI and sex. Rank correlations were considered low ($r < 0.5$), moderate ($0.5 < r < 0.7$) and high ($r \geq 0.7$) [39]. Multiple linear regression (MLR) analyses of SWA measurements as a function of steatosis, inflammation, ballooning and fibrosis were performed. Spearman's r values, regression coefficients, standard errors, 95% confidence intervals (CIs) and adjusted R^2 values were reported for each technique.

The diagnostic performance of MRI-PDFF, SWA and SWD for grading liver steatosis was evaluated with the receiver operating characteristic (ROC) curve. The optimal cutoff thresholds of SWA were calculated using Youden's index [40,41]. Areas under the curve (AUCs) were compared using the Delong method [42]. ROC curves of SWA for grading steatosis were also plotted for histopathology and MRI-PDFF as the reference standard. Thresholds for assessing steatosis grades using MRI-PDFF were fixed at 6.4%, 17.4% and 22.1%, according to Tang et al. [16]. All statistical tests were performed with software R (Version x64 4.2.1, R Foundation). The level of statistical significance was fixed at $p < 0.05$.

Results

Among 49 enrolled participants (24 females and 25 males), 13 were healthy volunteers and 36 had NAFLD or NASH. The mean age was 50.3 y (range: 25.8–71.0 y) for women and 56.0 y (range: 27.7–76.6 y) for men. Cohort characteristics are provided in Table 1. Four patients had only experimental US scans as they were excluded from MRI because of COVID-19, MRI non-compatibility with implants and claustrophobia. Thirteen healthy volunteers were included and were considered to have no steatosis, fibrosis, inflammation or ballooning (US and MRI scans but no biopsy). Representative examples of B-mode images and corresponding SWA maps are provided in Figure 2. SWA versus MRI-PDFF values are presented in Figure 3.

Shear wave attenuation and histopathological classification

The relationships between SWA and histology grades and stages are shown in Figure 4. SWA for steatosis grades S0 to S3 were 0.75 ± 0.22, 1.23 ± 0.15, 1.55 ± 0.10 and 1.79 ± 0.30 Np/m/Hz ($p < 0.001$). There were significant differences between S0 and other steatosis grades (S0 vs. S1, S0 vs. S2 and S0 vs. S3) and between S1 and S3 ($p < 0.001$).

Shear wave attenuation for lobular inflammation grades I0 to I3 were 0.81 ± 0.26, 1.53 ± 0.36, 1.70 ± 0.26 and 1.71 ± 0.26 Np/m/Hz

Table 1
Characteristics of the 49 participants

Characteristic	Results
Sex	
Men	25 (51%)
Women	24 (49%)
Age (y)	
Mean ± SD (range)	53.0 ± 15.2 (25.8–76.6)
BMI (kg/m^2)	
Mean ± SD (range)	
Non-NAFLD volunteers	[22.5 ± 1.8] (18.8–24.8)
NAFLD patients	[27.8 ± 5.4] (16.3–39.3)
Steatosis grade	
0	13 (26.5%)
1	10 (20.4%)
2	8 (16.3%)
3	18 (36.7%)
Lobular inflammation grade	
0	15 (30.6%)
1	20 (40.8%)
2	7 (14.3%)
3	7 (14.3%)
Hepatocellular ballooning grade	
0	16 (32.6%)
1	21 (42.9%)
2	12 (24.5%)
Fibrosis stage	
0	15 (30.6%)
1	9 (18.4%)
2	6 (12.2%)
3	9 (18.4%)
4	10 (20.4%)

Values in parentheses are percentages or ranges. Steatosis grade, lobular inflammation grade, hepatocellular ballooning grade and fibrosis stage were presumed to be 0 for the 13 healthy volunteers without steatosis.
BMI, body mass index; NAFLD, non-alcoholic fatty liver disease; SD, standard deviation.

($p < 0.001$), respectively. Mean values of SWA were differed significantly between I0 and I1 ($p < 0.001$), I0 and I2 ($p < 0.001$) and I0 and I3 ($p < 0.001$).

Shear wave attenuation for ballooning grades B0 to B2 were 0.86 ± 0.32, 1.62 ± 0.35 and 1.57 ± 0.31 Np/m/Hz ($p < 0.001$), respectively. B0 values statistically significantly differed from B1 ($p < 0.001$) and B2 ($p < 0.001$) values.

Shear wave attenuation for fibrosis stages F0 to F4 were 0.93 ± 0.53, 1.72 ± 0.32, 1.66 ± 0.26, 1.50 ± 0.32 and 1.37 ± 0.25 Np/m/Hz ($p < 0.001$), respectively. Values of SWA significantly differed between F0 and F1 ($p < 0.001$), F0 and F2 ($p < 0.05$) and F0 and F3 ($p < 0.05$).

Univariate and multivariate analyses

Linear regressions and R^2 and p values of SWA are reported in Table 2. All relationships with steatosis, lobular inflammation, ballooning and fibrosis were statistically significant ($0.11 \leq R^2 \leq 0.77$, $p \leq 0.03$). On the basis of Spearman's correlations (Table 3), relationships between SWA and steatosis, inflammation, ballooning and fibrosis were also significant ($0.31 \leq r \leq 0.89$, $p \leq 0.03$). Age and BMI were also correlated with SWA ($p \leq 0.03$). NASH variables with low Spearman correlations ($r < 0.5$) were neglected in MLR analyses. In MLR models, only SWA was correlated with steatosis grades ($p < 0.001$), with a high determination coefficient ($R^2 = 0.77$).

Diagnostic performance

Estimates of the diagnostic performance of MRI-PDFF, SWA and SWD in grading liver steatosis (ROC analyses) are illustrated in Figure 5. For differentiating S0 from ≥S1, there were no significant differences between AUCs of MRI-PDFF, SWA and SWD (respectively 0.97, 0.99 and 0.94). For differentiating S1 from ≥S2, AUCs were similar for MRI-PDFF and SWA (0.94 vs. 0.98), but significantly higher for SWA than SWD (0.98 vs. 0.78, $p = 0.001$) and significantly higher for MRI-PDFF than

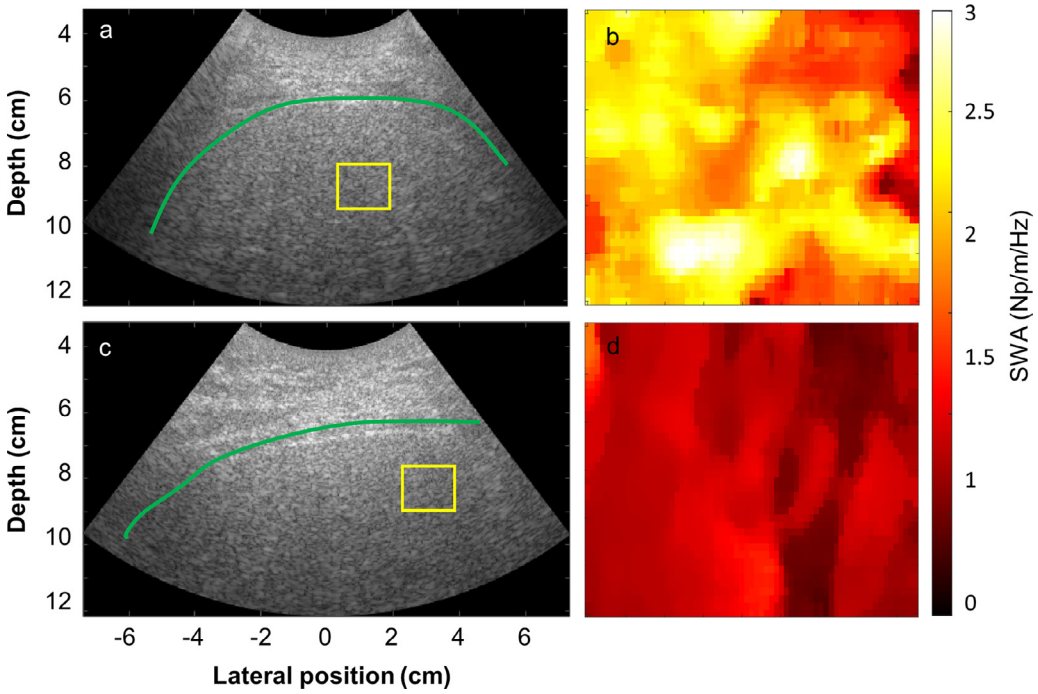

Figure 2. (a, b) Liver B-mode image (a) and SWA map (b) of a 45-y-old man with steatosis grade 3, lobular inflammation grade 2, ballooning grade 1, fibrosis stage 2 and an MRI-PDFF of 37.8%. (c, d) Liver B-mode image (c) and SWA map (d) of a 27-y-old healthy female volunteer with an MRI-PDFF of 2.1%. Liver boundaries and regions of interest of SWA maps are represented by the *green line* and the *yellow box* on B-mode images, respectively. MRI-PDFF, magnetic resonance imaging proton density fat fraction; SWA, shear wave attenuation.

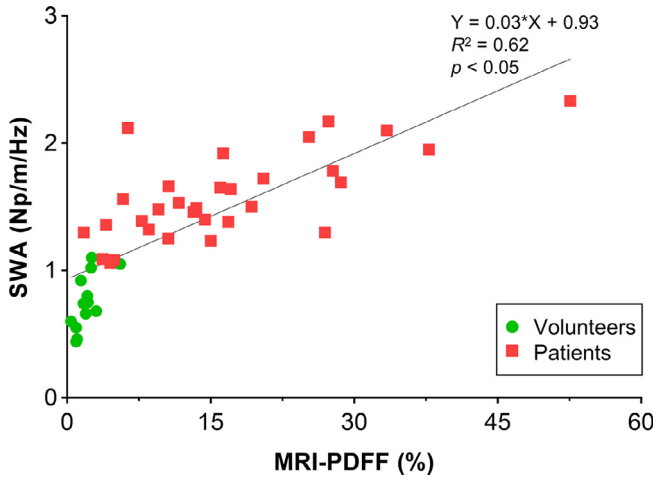

Figure 3. Scatterplot of SWA (Np/m/Hz) versus MRI-PDFF (%). MRI-PDFF, magnetic resonance imaging proton density fat fraction; SWA, shear wave attenuation.

SWD (0.94 vs. 0.78, $p = 0.01$). For differentiating ≤S2 from ≥S3, AUCs were similar for MRI-PDFF and SWA (0.90 vs. 0.93), but significantly higher for SWA than SWD (0.93 vs. 0.68, $p = 0.002$) and significantly higher for MRI-PDFF than SWD (0.90 vs. 0.68, $p = 0.01$).

Receiver operating characteristic curves of SWA for grading steatosis were also plotted for histopathology and MRI-PDFF as the reference standard (Fig. 6). With histopathology as reference, SWA had AUCs of 0.99 for differentiating S0 from ≥S1, 0.98 for differentiating ≤S1 from ≥S2 and 0.93 for differentiating ≤S2 from S3. With MRI-PDFF as reference, SWA had AUCs of 0.92 for differentiating S0 from ≥S1, 0.91 for differentiating ≤S1 from ≥S2 and 0.91 for differentiating ≤S2 from S3. SWA Youden thresholds for steatosis grading are reported in Table 4. Optimal SWA thresholds for grading steatosis were respectively 1.05, 1.37 and 1.51 Np/m/Hz for S0 versus ≥S1, ≤S1 versus ≥S2 and ≤S2 versus S3 using biopsy as the reference standard, and respectively 1.16, 1.49 and 1.67 Np/m/Hz when using MRI-PDFF as the reference standard.

Discussion

In this prospective pilot study, SWA imaging was investigated as a biomarker for assessing hepatic steatosis, lobular inflammation, ballooning and fibrosis. Histopathology was used as the reference standard. Liver biopsy specimens were evaluated according to the NASH CRN Pathology Committee using the NAFLD histology scoring system.

On univariate analysis, SWA had low to high correlations with liver steatosis, lobular inflammation, ballooning scores and fibrosis. However, on multivariate regression, only SWA was strongly correlated with liver steatosis. As liver lobular inflammation was close to the statistically significant level ($p = 0.053$), a definite correlation between SWA and lobular inflammation might appear in a larger cohort study. SWA provided high diagnostic performance for classification of dichotomized steatosis grades. We then computed SWA cutoff thresholds for differentiating steatosis grades, using either biopsy or MRI-PDFF as the reference standard. The use of SWA to assess liver steatosis was recently evaluated in a few clinical cases. Ormachea and Parker [27] and Sharma et al. [31] reported a moderate correlation between SWA and steatosis grades (Spearman's $r = 0.52$ and $r = 0.69$, respectively). The higher correlation observed in our study ($r = 0.90$) may be explained by the larger number of study participants and the inclusion of healthy volunteers, which provides a broader spectrum of liver conditions. Moreover, in their studies, SWA were computed with a different algorithm at a single frequency.

Because MRI-PDFF and SWD were previously reported to be correlated with steatosis grade [15,17,27,28,43], we compared the performance of SWA with that of those biomarkers in the current study. On the basis of ROC AUCs, we could determine that SWA and MRI-PDFF performed better than SWD and that SWA and MRI-PDFF performed similarly. The latter observation constitutes a significant advance when considering the value of MRI-PDFF as an alternative reference standard to biopsy for assessing liver steatosis [16,38,44–46].

One of the aforementioned studies compared the diagnostic performance of SWA and SWD. Ormachea and Parker [27] found that the SWA-AUC for steatosis detection (S0 vs. ≥S1) was higher than that for SWD. On the other hand, AUCs of SWA and SWD were similar for grading the steatosis severity (S1 vs. S2 and ≤S2 vs. S3) [27], whereas we found that SWA provided higher performance than SWD for all steatosis grades. Differences between both studies may again be attributed to the algorithm and the frequencies considered for computing SWA. In our study, SWA was based on a gamma fitting on the whole available frequency bandwidth (0–1000 Hz), whereas in Ormachea and Parker [27], it was assessed at a fixed frequency of 150 Hz. This is relevant because the chosen frequency bandwidth is known to influence SWA computation [47]. Some studies on SWA reported results at a single frequency [27,31] or in a range of frequencies [33,48–51].

The frequency range is also a source of variation for SWD. Bandwidths from 30 to 450 Hz were reported for liver imaging [28,29,36]. In the current study, the selected bandwidth (67–110 Hz) was within reported ranges and was kept constant for all data sets. To reduce the

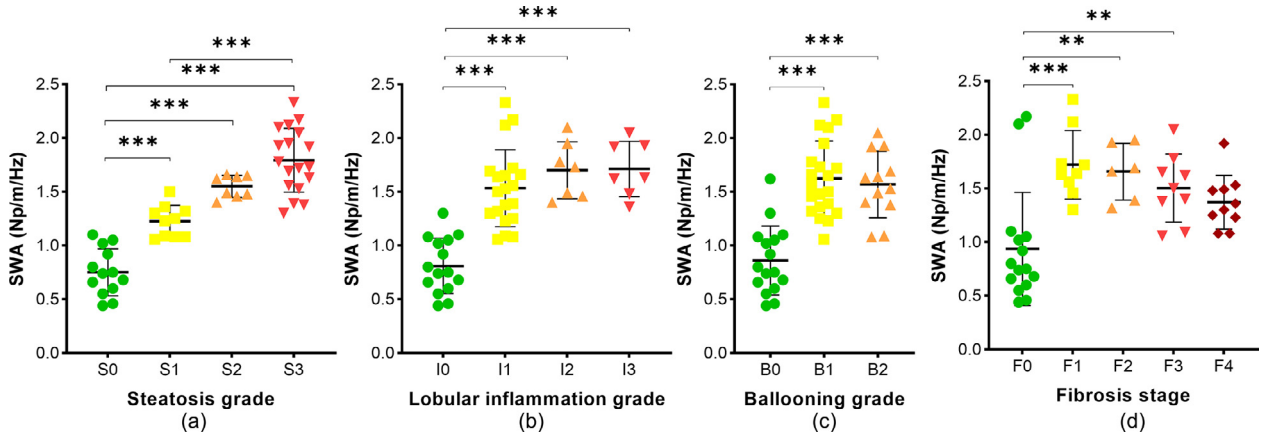

Figure 4. Scatterplots, means and standard deviations of SWA for different grades of (a) steatosis, (b) lobular inflammation, (c) ballooning and (d) fibrosis. *$p < 0.05$, **$p < 0.01$, ***$p < 0.001$. SWA, shear wave attenuation.

Table 2
SWA for different grades of steatosis, lobular inflammation, ballooning and fibrosis and linear regressions of SWA with respect to biopsy grade

Histopathological grade or stage	Shear wave attenuation (Np/m/Hz, mean ± SD)			
	Steatosis	Inflammation	Ballooning	Fibrosis
0	0.75 ± 0.22	0.81 ± 0.26	0.86 ± 0.32	0.93 ± 0.53
1	1.23 ± 0.15	1.53 ± 0.36	1.62 ± 0.35	1.72 ± 0.32
2	1.55 ± 0.10	1.70 ± 0.26	1.57 ± 0.31	1.66 ± 0.26
3	1.79 ± 0.30	1.71 ± 0.26	—	1.50 ± 0.32
4	—	—	—	1.37 ± 0.25
Linear regression	$0.34x + 0.81$ ($R^2 = 0.77$, $p < 0.001$)	$0.32x + 1.01$ ($R^2 = 0.44$, $p < 0.001$)	$0.38x + 1.01$ ($R^2 = 0.36$, $p < 0.001$)	$0.11x + 1.19$ ($R^2 = 0.11$, $p = 0.03$)

Table 3
Univariate and multivariate linear regression analyses of shear wave attenuation versus liver histopathology grades, age, sex and body mass index

	Univariate analysis			Multiple linear regression analysis			
	Spearman's *r*	95% CI	*P* Value	Estimated coefficient	95% CI	*P* Value	Adjusted R^2
Steatosis	0.89	0.80, 0.94	<0.001	0.32	0.23, 0.40	<0.001	0.77
Lobular inflammation	0.73	0.56, 0.84	<0.001	0.09	−0.01, 0.19	0.053	
Ballooning	0.62	0.40, 0.77	<0.001	−0.06	−0.20, 0.07	0.334	
Fibrosis	0.31	0.03, 0.55	0.03	—	—	—	
Age (y)	0.32	0.04, 0.56	0.03	—	—	—	
Body mass index (kg/m^2)	0.36	0.08, 0.59	0.01	—	—	—	
Sex	0.11	−0.19, 0.38	0.48	—	—	—	

impact of outliers (*i.e.*, variability in shear wave velocity with frequency), the A-RANSAC method was used to improve the robustness of SWD computations. The A-RANSAC applied on gamma fitting parameters of frequency spectra was also used for SWA analyses.

To differentiate histologically determined steatosis grades with SWA, we computed thresholds that maximized the Youden index. We observed good sensitivity (0.83–1.00) and high specificity (0.87–0.96) in differentiation of steatosis grades. When biopsy was used as the reference standard, SWA provided higher sensitivity than MRI-PDFF and the same range of specificity as reported in previous studies [15,16]. If independently validated in larger cohorts, SWA may constitute an alternative to MRI-PDFF because of its potential implementation on US scanners, cost-effectiveness and availability as a point-of-care tool for screening of liver steatosis.

Quantitative US (QUS) methods that have been investigated as alternative approaches to biopsy for assessment of liver steatosis have also attracted some attention. Recent studies have evaluated the compression wave attenuation coefficient [52], backscatter coefficient [53] or both attenuation and backscatter coefficients [54] for assessment of steatosis. One limitation of these QUS-based methods is their dependency on reference phantoms for calibrations, but some efforts have been made to overcome this issue [54,55]. In a recent study involving patients with NAFLD across multiple centers, the effectiveness of multiparametric US was evaluated using various techniques, including attenuation imaging (ATI) to measure the compression wave attenuation coefficient, as well as 2-D SWE to assess liver stiffness and the dispersion slope [52]. However, further head-to-head comparisons of performance between the most recent SWA technologies and QUS-based techniques on the same patients remain to be performed in future studies.

This study has some limitations. First, because of the relatively small number of patients in this pilot study, some combinations of histopathological features were not available (*e.g.*, a patient with S0 and >F1 or a patient with F0 and S2). Therefore, the diagnostic performance assessment might not have considered the whole spectrum encountered in

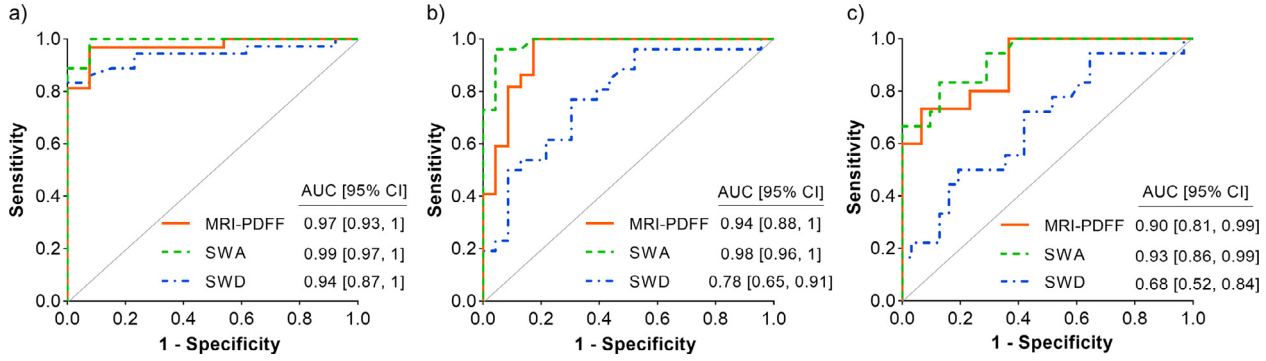

Figure 5. Receiver operating characteristic curves of MRI-PDFF, SWA and SWD for dichotomization of (a) stage 0 versus ≥stage 1, (b) ≤stage 1 versus ≥stage 2 and (c) ≤stage 2 versus stage 3 using histopathological grading as the reference standard. AUC, area under the receiver operating characteristic curve; CI, confidence interval; MRI-PDFF, magnetic resonance imaging proton density fat fraction; SWA, shear wave attenuation; SWD, shear wave dispersion; US, ultrasound.

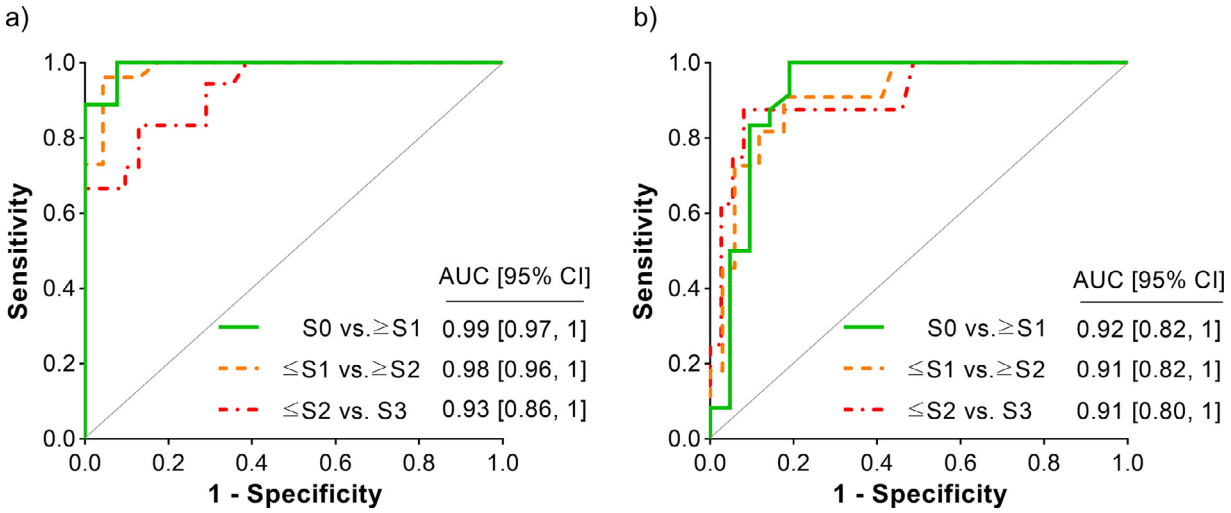

Figure 6. Receiver operating characteristic curves of SWA for grading liver steatosis using (a) histopathology and (b) magnetic resonance imaging proton density fat fraction as the reference standard. AUC, area under the receiver operating characteristic curve; CI, confidence interval.

Table 4
Shear wave attenuation optimal cutoff values and associated sensitivity, specificity, PPV and NPV for different steatosis grades using biopsy and MRI-PDFF as the reference standard

Steatosis grade	AUC [95% CI]	Cutoff (Np/m/Hz)	Sensitivity [95% CI]	Specificity [95% CI]	PPV [95% CI]	NPV [95% CI]	Accuracy [95 % CI]	*F*1-score [95% CI]
Reference standard: biopsy								
S0 vs. ≥S1	0.99 [0.97, 1]	1.05	1.00 [0.90, 1]	0.92 [0.67, 1]	0.97 [0.86, 1]	1.00 [0.74, 1]	0.98 [0.89, 1]	0.99 [0.92,1]
≤S1 vs. ≥S2	0.98 [0.96, 1]	1.37	0.96 [0.81, 1]	0.96 [0.79, 1]	0.96 [0.80, 1]	0.96 [0.78, 1]	0.96 [0.86, 0.99]	0.96 [0.86, 0.99]
≤S2 vs. S3	0.93 [0.86, 1]	1.51	0.83 [0.59, 0.96]	0.87 [0.70, 0.96]	0.79 [0.54, 0.94]	0.90 [0.74, 0.98]	0.86 [0.73, 0.94]	0.81 [0.61, 0.93]
Reference standard: MRI-PDFF								
S0 vs. ≥S1	0.92 [0.82, 1]	1.16	1.00 [0.86, 1]	0.81 [0.60, 0.92]	0.86 [0.67, 0.96]	1.00 [0.81, 1]	0.91 [0.79, 0.98]	0.92 [0.80, 0.98]
≤S1 vs. ≥S2	0.91 [0.82, 1]	1.49	0.91 [0.62, 0.99]	0.82 [0.66, 0.92]	0.63 [0.35, 0.85]	0.96 [0.82, 1]	0.84 [0.70, 0.93]	0.74 [0.53, 0.90]
≤S2 vs. S3	0.91 [0.80, 1]	1.67	0.87 [0.53, 0.99]	0.92 [0.79, 0.97]	0.70 [0.35, 0.93]	0.97 [0.85, 1]	0.91 [0.79, 0.98]	0.78 [0.47, 0.96]

AUC, area under the receiver operating characteristic curve; CI, confidence interval; MRI-PDFF, magnetic resonance imaging proton density fat fraction; NPV, negative predictive value; PPV, positive predictive value.

NASH. Second, as there were no SWA thresholds published in the literature for liver steatosis grading, it was not possible to compare our results with prior results. Third, because steatosis, inflammation, ballooning and fibrosis are all correlated with SWA, these histopathological features may confound the interpretation of SWA for steatosis grading. However, the strongest association was observed in the presence of steatosis. Future work on larger cohorts will be required to systematically address these potential confounders of SWA. Finally, the interval between biopsy and US or MRI measurements was 37.8 ± 34.6 d. SWA accuracy for NASH assessment may be improved by using a smaller interval between biopsy, US and MR imaging [15].

Conclusion

This pilot, prospective, cross-sectional study in a cohort of volunteers and patients with biopsy-confirmed NAFLD or NASH determined the feasibility of using SWA as a non-invasive biomarker for early detection of hepatic steatosis with high sensitivity and specificity. Also, SWA provided excellent accuracy for classification of moderate and severe steatosis grades, whether considering biopsy or MRI-PDFF as the reference standard in this pilot study. These results are meant to illustrate the feasibility of the SWA parameter as a biomarker, and with a larger cohort, cutoff values might likely be modified. Prospective studies with larger cohorts will help validate the diagnostic performance of SWA for non-invasive detection and grading of liver steatosis.

Acknowledgments

This work was supported in part by the Natural Sciences and Engineering Research Council of Canada under Grant 2022-03729, in part by the Canadian Institutes of Health Research under Grant 389385 and in part by the Oncotech Consortium (Oncopole, Medteq, Transmedtech, Cancer Research Society, Fonds de Recherche Santé du Québec and Siemens Healthcare) under Grant 293741. Salary award by the Fonds de recherche du Québec en Santé and Fondation de l'association des radiologistes du Québec (FRQS-FARQ #298509) was obtained by An Tang. Giada Sebastiani is supported by a Senior Salary Award from FRQS (No. 296306).

We thank Dr. Marie-Hélène Roy-Cardinal for her guidance in statistical analysis and Mr. Miloud Zenati for his assistance in patient enrollment and data collection.

Conflict of interest

G.S. has acted as speaker for Pfizer, Merck, Novo Nordisk, Novartis, Gilead and AbbVie; has served as an advisory board member for Merck,

Gilead, Pfizer, Allergan, Novo Nordisk, Intercept and Novartis; and has received unrestricted research funding from Thera technologies Inc. A. T. and G.C. have received equipment loans and funding from Siemens Healthcare.

Data availability statement

Clinical ultrasound radiofrequency data sets might be available on request for collaborative works. A data sharing agreement might be requested by the University of Montreal Hospital Research Center to respect institutional and governmental regulations.

Supplementary materials

Supplementary material associated with this article can be found in the online version at doi:10.1016/j.ultrasmedbio.2023.06.020.

References

[1] Mitra S, De A, Chowdhury A. Epidemiology of non-alcoholic and alcoholic fatty liver diseases. Transl Gastroenterol Hepatol 2019;5:16–33.
[2] Ofosu A, Ramai D, Reddy M. Non-alcoholic fatty liver disease: controlling an emerging epidemic, challenges, and future directions. Ann Gastroenterol 2018;31:288–95.
[3] Adams LA, Lindor KD. Nonalcoholic fatty liver disease. Ann Epidemiol 2007;17:863–9.
[4] Zhang JZ, Cai JJ, Yu Y, She ZG, Li H. Nonalcoholic fatty liver disease: an update on the diagnosis. Gene Expr 2019;19:187–98.
[5] McPherson S, Hardy T, Henderson E, Burt AD, Day CP, Anstee QM. Evidence of NAFLD progression from steatosis to fibrosing-steatohepatitis using paired biopsies: implications for prognosis and clinical management. J Hepatol 2015;62:1148–55.
[6] Gaidos JK, Hillner BE, Sanyal AJ. A decision analysis study of the value of a liver biopsy in nonalcoholic steatohepatitis. Liver Int 2008;28:650–8.
[7] Colloredo G, Guido M, Sonzogni A, Leandro G. Impact of liver biopsy size on histological evaluation of chronic viral hepatitis: the smaller the sample, the milder the disease. Hepatology 2003;39:239–44.
[8] Kleiner DE, Brunt EM, Van Natta M, Behling C, Contos MJ, Cummings OW, et al. Design and validation of a histological scoring system for nonalcoholic fatty liver disease. J Hepatol 2005;41:1313–21.
[9] Myers RP, Fong A, Shaheen AA. Utilization rates, complications and costs of percutaneous liver biopsy: a population-based study including 4275 biopsies. Liver Int 2008;28:705–12.
[10] Noureddin M, Loomba R. Nonalcoholic fatty liver disease: indications for liver biopsy and noninvasive biomarkers. Clin Liver Disease (Hoboken) 2012;1:104–7.
[11] Sumida Y, Nakajima A, Itoh Y. Limitations of liver biopsy and non-invasive diagnostic tests for the diagnosis of nonalcoholic fatty liver disease/nonalcoholic steatohepatitis. World J Gastroenterol 2014;20:475–85.
[12] Kramer H, Pickhardt PJ, Kliewer MA, Hernando D, Chen GH, Zagzebski JA, et al. Accuracy of liver fat quantification with advanced CT, MRI, and ultrasound techniques: prospective comparison with MR spectroscopy. AJR Am J Roentgenol 2017;208:92–100.
[13] Mehta SR, Thomas EL, Bell JD, Johnston DG, Taylor-Robinson SD. Non-invasive means of measuring hepatic fat content. World J Gastroenterol 2008;14:3476–83.
[14] Qayyum A, Chen DM, Breiman RS, Westphalen AC, Yeh BM, Jones KD, et al. Evaluation of diffuse liver steatosis by ultrasound, computed tomography, and magnetic resonance imaging: which modality is best? Clin Imaging 2009;33:110–5.
[15] Tang A, Tan J, Sun M, Hamilton G, Bydder M, Wolfson T, et al. Nonalcoholic fatty liver disease: MR imaging of liver proton density fat fraction to assess hepatic steatosis. Radiology 2013;267:422–31.
[16] Tang A, Desai A, Hamilton G, Wolfson T, Gamst A, Lam J, et al. Accuracy of MR imaging-estimated proton density fat fraction for classification of dichotomized histologic steatosis grades in nonalcoholic fatty liver disease. Radiology 2015;274:416–25.
[17] Ferraioli G, Berzigotti A, Barr RG, Choi BI, Cui XW, Dong Y, et al. Quantification of liver fat content with ultrasound: a WFUMB position paper. Ultrasound Med Biol 2021;47:2803–20.
[18] Kalra N, Duseja A, Das A, Dhiman RK, Virmani V, Chawla Y, et al. Chemical shift magnetic resonance imaging is helpful in detecting hepatic steatosis but not fibrosis in patients with nonalcoholic fatty liver disease (NAFLD). Ann Hepatol 2009;8:21–5.
[19] Lin SC, Heba E, Wolfson T, Ang B, Gamst A, Han A, et al. Noninvasive diagnosis of nonalcoholic fatty liver disease and quantification of liver fat using a new quantitative ultrasound technique. Clin Gastroenterol Hepatol 2015;13 1337–45.e6.
[20] Smith-Bindman R, Lipson J, Marcus R, Kim KP, Mahesh M, Gould R, et al. Radiation dose associated with common computed tomography examinations and the associated lifetime attributable risk of cancer. Arch Intern Med 2009;169:2078–86.
[21] Strauss S, Gavish E, Gottlieb P, Katsnelson L. Interobserver and intraobserver variability in the sonographic assessment of fatty liver. Am J Roentgenology 2007;189 W320–W3.
[22] Khov N, Sharma A, Riley TR. Bedside ultrasound in the diagnosis of nonalcoholic fatty liver disease. World J Gastroenterol 2014;20:6821–5.
[23] Zhang YN, Fowler KJ, Hamilton G, Cui JY, Sy EZ, Balanay M, et al. Liver fat imaging—a clinical overview of ultrasound, CT, and MR imaging. Br J Radiol 2018;91:20170959.
[24] Zwiebel WJ. Sonographic diagnosis of diffuse liver disease. Semin Ultrasound CT MR 1995;16:8–15.
[25] Li H, Flé G, Bhatt M, Qu Z, Ghazavi S, Yazdani L, et al. Viscoelasticity imaging of biological tissues and single cells using shear wave propagation. Front Phys 2021;9:350.
[26] Barr RG, Ferraioli G, Palmeri ML, Goodman ZD, Garcia-Tsao G, Rubin J, et al. Elastography assessment of liver fibrosis: Society of Radiologists in Ultrasound Consensus Conference Statement. Radiology 2015;27:845–61.
[27] Ormachea J, Parker KJ. Comprehensive viscoelastic characterization of tissues and the inter-relationship of shear wave (group and phase) velocity, attenuation and dispersion. Ultrasound Med Biol 2020;46:3448–59.
[28] Barry CT, Mills B, Hah Z, Mooney RA, Ryan CK, Rubens DJ, et al. Shear wave dispersion measures liver steatosis. Ultrasound Med Biol 2012;38:175–82.
[29] Bhatt M, Yazdani L, Destrempes F, Allard L, Nguyen BN, Tang A, et al. Multiparametric in vivo ultrasound shear wave viscoelastography on farm-raised fatty duck livers: human radiology imaging applied to food sciences. Poult Sci 2021;100:100968.
[30] Gesnik M, Bhatt M, Roy Cardinal MH, Destrempes F, Allard L, Nguyen BN, et al. In vivo ultrafast quantitative ultrasound and shear wave elastography imaging on farm-raised duck livers during force feeding. Ultrasound Med Biol 2020;46:1715–26.
[31] Sharma AK, Reis J, Oppenheimer DC, Rubens DJ, Ormachea J, Hah Z, et al. Attenuation of shear waves in normal and steatotic livers. Ultrasound Med Biol 2019;45:895–901.
[32] Nenadic IZ, Urban MW, Heng Z, Sanchez W, Morgan PE, Greenleaf JF, et al. Application of attenuation measuring ultrasound shearwave elastography in 8 post-transplant liver patients. Proc IEEE Int Ultrason Symp 2014:987–90.
[33] Yazdani L, Bhatt M, Rafati I, Tang A, Cloutier G. The revisited frequency-shift method for shear wave attenuation computation and imaging. IEEE Trans Ultrason Ferroelectr Freq Control 2022;69:2061–74.
[34] Garcia D, Tarnec LL, Muth S, Montagnon E, Porée J, Cloutier G. Stolt's f-k migration for plane wave ultrasound imaging. IEEE Trans Ultrason Ferroelectr Freq Control 2013;60:1853–67.
[35] Loupas T, Peterson RB, Gill RW. Experimental evaluation of velocity and power estimation for ultrasound blood flow imaging, by means of a two-dimensional autocorrelation approach. IEEE Trans Ultrason Ferroelectr Freq Control 1995;42:689–99.
[36] Parker KJ, Partin A, Rubens DJ. What do we know aout shear wave dispersion in normal and steatotic livers? Ultrasound Med Biol 2015;41:1481–7.
[37] Longo R, Pollesello P, Ricci C, Masutti F, Kvam BJ, Bercich L, et al. Proton MR spectroscopy in quantitative in vivo determination of fat content in human liver steatosis. J Magn Reson Imaging 1995;5:281–5.
[38] Tang A, Dzyubak B, Yin M, Schlein A, Henderson WC, Hooker JC, et al. MR elastography in nonalcoholic fatty liver disease: inter-center and inter-analysis-method measurement reproducibility and accuracy at 3T. Eur Radiol 2022;32:2937–48.
[39] Mukaka MM. Statistics corner: a guide to appropriate use of correlation coefficient in medical research. Malawi Med J 2012;24:69–71.
[40] Youden WJ. Index for rating diagnostic tests. Cancer 1950;3:32–5.
[41] Rota M, Antolini L, Valsecchi MG. Optimal cut-point definition in biomarkers: the case of censored failure time outcome. BMC Med Res Methodol 2015;15:24.
[42] DeLong ER, DeLong DM, Clarke-Pearson DL. Comparing the areas under two or more correlated receiver operating characteristic curves: a nonparametric approach. Biometrics 1988;44:837–45.
[43] Zhang XQ, Zheng RQ, Jin JY, Wang JF, Zhang T, Zeng J. US shear-wave elastography dispersion for characterization of chronic liver disease. Radiology 2022;305:597–605.
[44] Qi Q, Weinstock AK, Chupetlovska K, Borhani AA, Jorgensen DR, Furlan A, et al. Magnetic resonance imaging-derived proton density fat fraction (MRI-PDFF) is a viable alternative to liver biopsy for steatosis quantification in living liver donor transplantation. Clin Transplant 2021;35:e14339.
[45] Ligabue G, Besutti G, Scaglioni R, Stentarelli C, Guaraldi G. MR quantitative biomarkers of non-alcoholic fatty liver disease: technical evolutions and future trends. Quant Imaging Med Surg 2013;3:192–5.
[46] Ferraioli G, Maiocchi L, Raciti MV, Tinelli C, De Silvestri A, Nichetti M, et al. Detection of liver steatosis with a novel ultrasound-based technique: a pilot study using MRI-derived proton density fat fraction as the gold standard. Clin Transl Gastroenterol 2019;10:e00081.
[47] Parker KJ, Ormachea J, Drage MG, Kim H, Hah Z. The biomechanics of simple steatosis and steatohepatitis. Phys Med Biol 2018;63:105013.
[48] Budelli E, Brum J, Bernal M, Deffieux T, Tanter M, Lema P, et al. A diffraction correction for storage and loss moduli imaging using radiation force based elastography. Phys Med Biol 2017;62:91–106.
[49] Nenadic IZ, Qiang B, Urban MW, Zhao H, Sanchez W, Greenleaf JF, et al. Attenuation measuring ultrasound shearwave elastography and in vivo application in post-transplant liver patients. Phys Med Biol 2017;62:484–500.
[50] Bernard S, Kazemirad S, Cloutier G. A frequency-shift method to measure shear-wave attenuation in soft tissues. IEEE Trans Ultrason Ferroelectr Freq Control 2017;64:514–24.
[51] Kijanka P, Urban MW. Two-point frequency shift method for shear wave attenuation measurement. IEEE Trans Ultrason Ferroelectr Freq Control 2020;67:483–96.

[52] Jang JK, Lee ES, Seo JW, Kim YR, Kim SY, Cho YY, et al. Two-dimensional shear-wave elastography and US attenuation imaging for nonalcoholic steatohepatitis diagnosis: across-sectional, multicenter study. Radiology 2022;305:118–26.
[53] Wear KA, Han A, Rubin JM, Gao J, Lavarello R, Cloutier G, et al. US Backscatter for liver fat quantification: an AIUM-RSNA QIBA Pulse-Echo quantitative ultrasound initiative. Radiology 2022;305:526–37.
[54] Labyed Y, Milkowski A. Novel method for ultrasound-derived fat fraction using an integrated phantom. J Ultrasound Med 2020;39:2427–38.
[55] Rafati I, Destrempes F, Yazdani L, Gesnik M, Tang A, Cloutier G. Regularized ultrasound phantom-free local attenuation coefficient slope (ACS) imaging in homogeneous and heterogeneous tissues. IEEE Trans Ultrason Ferroelectr Freq Control 2022;69:3338–52.